Supplement of Atmos. Chem. Phys., 23, 5679–5697, 2023
https://doi.org/10.5194/acp-23-5679-2023-supplement

Atmospheric Chemistry and Physics
Open Access
EGU

Supplement of

Impact of HO_2 aerosol uptake on radical levels and O_3 production during summertime in Beijing

Joanna E. Dyson et al.

Correspondence to: Lisa K. Whalley (l.k.whalley@leeds.ac.uk) and Dwayne E. Heard (d.e.heard@leeds.ac.uk)

S1.1 FAGE instrumentation description

The University of Leeds Fluorescence Assay by Gas Expansion (FAGE) instrument made measurements of OH, HO_2 and RO_2 radicals and OH reactivity (k_{OH}). The FAGE instrument set up is described fully in Whalley et al., 2018 while the OH reactivity instrument set up is described fully in Whalley et al., 2016. Both instruments are also described fully in Slater et al., 2020 and so only a brief description is given here.

Two cells, a HO_x cell and a RO_x cell connected together with a side arm, were used to take radical measurements from the roof of the Leeds FAGE lab container. A RO_xLIF flow reactor was also coupled to the RO_x cell to allow for detection of RO_2 (total, complex and simple) as described by Fuchs et al., 2008. The HO_x cell took sequential measurements of OH and the sum of OH and HO_2, by the addition of NO (Messer, 99.5 %), which titrated HO_2 to OH for detection by Laser Induced Fluorescence (LIF) at 308 nm.

The RO_xLIF reactor operated in 2 modes: a 'HO_x mode' where a flow of CO (10 % in N_2) was added to ambient sampled air close to the pin hole to convert all ambient OH to HO_2; and a 'RO_x mode' where NO (500 ppmv in N_2) was added in addition to the CO flow to convert all RO_2 into OH before all OH was then rapidly converted by CO into HO_2. The air from the RO_xLIF reactor was then drawn into the FAGE low pressure fluorescence cell, whereupon pure NO (Messer, 99.5 %) was injected to convert HO_2 to OH. In HO_x mode, the sum of OH, HO_2 and complex RO_2 was measured, while in RO_x mode, the sum of OH, HO_2 and total RO_2 was measured. From this the concentration of complex RO_2 and HO_2/OH from RO_x can be determined.

An Inlet Pre-Injector was used attached to the HO_x cell to remove ambient OH by injecting propane directly above the inlet of the cell. This leads to a background measurement while the laser is still online to the OH transition; this background is known as OH_{CHEM}. OH_{CHEM} includes signal from laser scatter and scattered solar radiation and any fluorescence signal from any OH generated inside the cell from an interference precursor. By comparing OH_{CHEM} to the signal generated when the 308 nm laser tuned off the OH transition, OH_{WAVE}, the contribution of any interference can be identified. While the laser is offline, OH_{WAVE}, any signal seen is from laser scattered light and scattered solar radiation. Agreement between OH_{WAVE} and OH_{CHEM} was generally very good during the Summer AIRPRO campaign with an overall orthogonal distance regression slope of 1.103 ± 0.017, with the exception of an interference seen when O_3 levels were elevated (see Woodward-Massey et al., 2020 for details).

S1.2 Correlation between aerosol surface area and NO_x mixing ratio

During winter haze periods in Beijing, a strong correlation has been observed between $PM_{2.5}$ and NO_x (Slater et al., 2020). During the Summer Beijing AIRPRO campaign in 2017, no strong correlation between $PM_{2.5}$ and NO_x was seen. A correlation plot of $PM_{2.5}$ aerosol surface area (cm^2 cm^{-3}) versus NO and NO_2 mixing ratio (ppb) is shown in Figure S1.

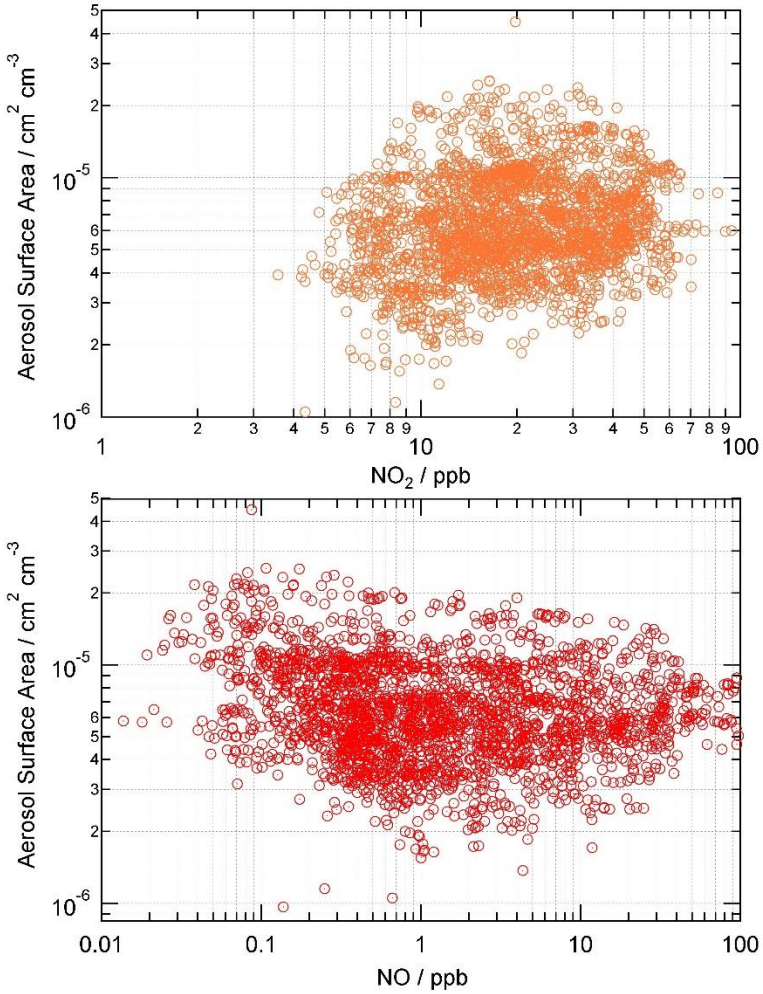

Figure S1. Correlation plot of $PM_{2.5}$ aerosol surface area (cm^2 cm^{-3}) versus NO_2 (orange circles) and NO (red circles) mixing ratio (ppb) for Summer Beijing Campaign.

S1.3 HO_2 measured:modelled dependence on NO mixing ratio

Figure S2 shows the ratio of measured to modelled OH, HO_2 and RO_2 radical concentrations binned against NO mixing ratio (ppb) for MCM_gamma, compared to MCM_base.

For the range of NO mixing ratios observed across the summer AIRPRO campaign, the OH measured to modelled ratio is close to 1 between ~0.3 and 2 ppb NO with the MCM_base model beginning to under-predict OH slightly both below 0.3 ppb NO and above 2 ppb NO. Both HO_2 and RO_2 radical concentrations were strongly dependent on NO mixing ratio, with the model over-predicting HO_2 below ~ 1 ppb NO. For the entire campaign the average NO was 4.7 ppb with 45% of NO measurements taken across campaign being less than or equal to 1 ppb. Across all NO mixing ratios the measured to modelled ratio for RO_2 shows a large under-prediction, with the largest under-prediction at the highest NO mixing ratios. This is likely contributing to the underprediction of HO_2 at higher NO mixing ratios. From Figure S2 it can be seen that the addition of the calculated HO_2 uptake coefficient has had little effect across the range of NO mixing ratios measured during the summer AIRPRO campaign.

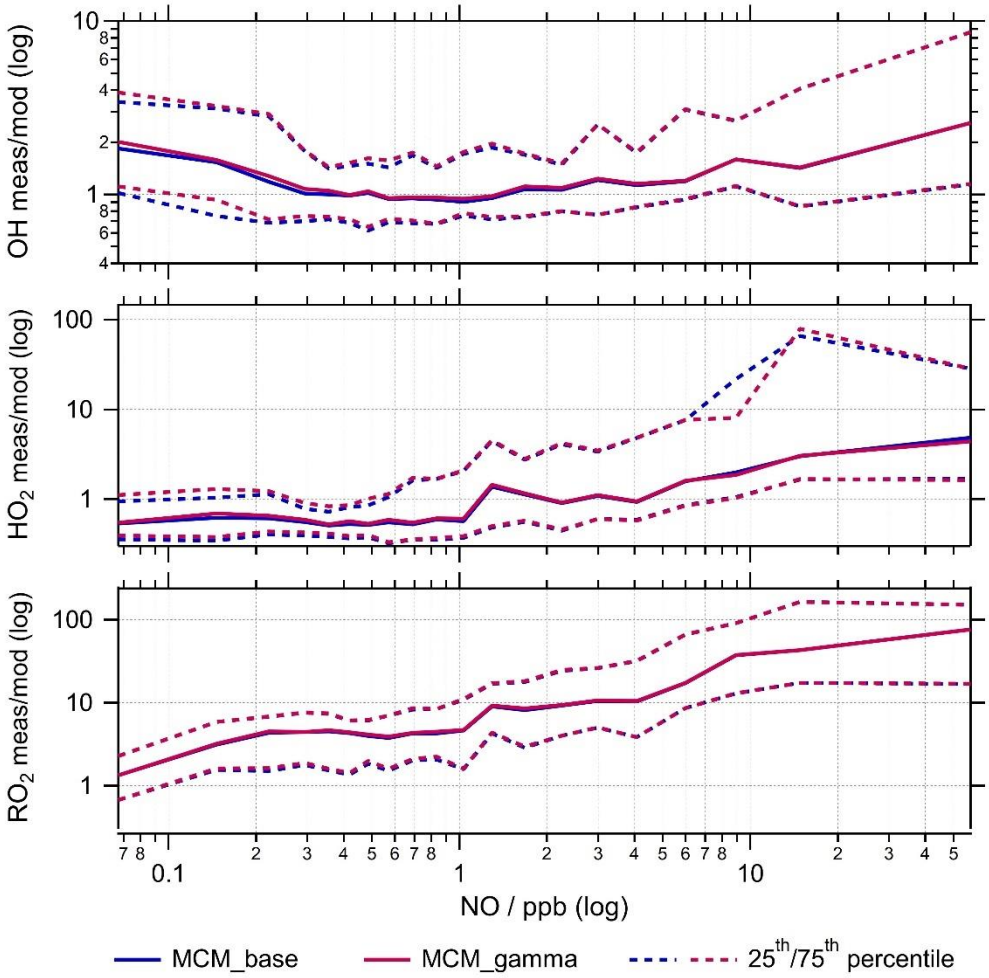

Figure S2. Ratio of measured to modelled OH, HO_2 and RO_2 radical concentrations using the MCM_base (blue) and MCM_gamma (dark pink) model binned over the range of NO mixing ratios (ppb) for the summer AIRPRO campaign. Solid lines show the median average measured to modelled radical concentration. Dashed lines show the $25^{th}/75^{th}$ percentiles.

As seen in Figure S3, the addition of γ_{HO_2} = 0.2 affected the ability of the model to reproduce the NO dependence of radical concentrations. While MCM_base over-predicts HO_2 below ~ 1 ppb NO, the over-prediction of HO_2 decreases below 1 ppb NO for MCM_SA with HO_2 being well reproduced at the lowest NO mixing ratios (i.e. < 0.1 ppb) due to the relative increase in the importance of HO_2 uptake as a sink of HO_2. Modelled RO_2 is not significantly affected by the addition of HO_2 uptake at any NO mixing ratio. The modelled concentration of OH is under-predicted for the entire range of NO mixing ratios compared to measured values, though only slightly between ~ 1 and 6 ppb NO. Below ~ 4 ppb NO, the underprediction of OH by MCM_SA increases compared to MCM_base due most likely to loss of HO_2 onto aerosols competing with loss via NO to give OH. Budget analysis done by Whalley et al., 2021, showcases that with a reduction in over-prediction of modelled HO_2, OH is under-predicted revealing a missing OH source.

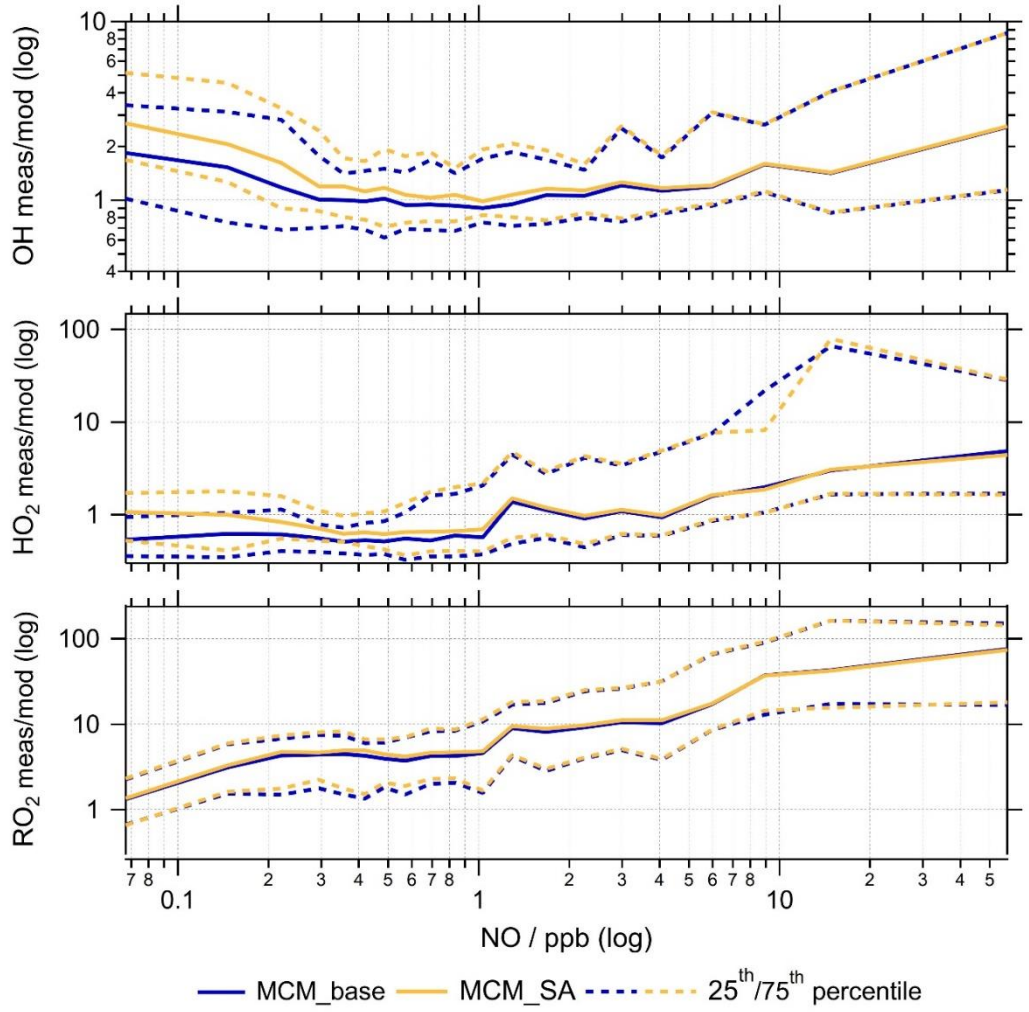

Figure S3. Ratio of measured to modelled OH, HO_2 and RO_2 radical concentrations using the MCM_base (blue) and MCM_SA (yellow) model binned over the range of NO mixing ratios (ppb) for the summer AIRPRO campaign. Solid lines show the median average measured to modelled radical concentration. Dashed lines show the $25^{th}/75^{th}$ percentile.

S1.4 HO_2 measured:modelled dependence on aerosol surface area

Figure S4**Figure** shows the ratio of measured to modelled HO_2 radical concentrations as a function of aerosol surface area concentration (cm^2 cm^{-3}) for the entire Summer AIRPRO campaign.

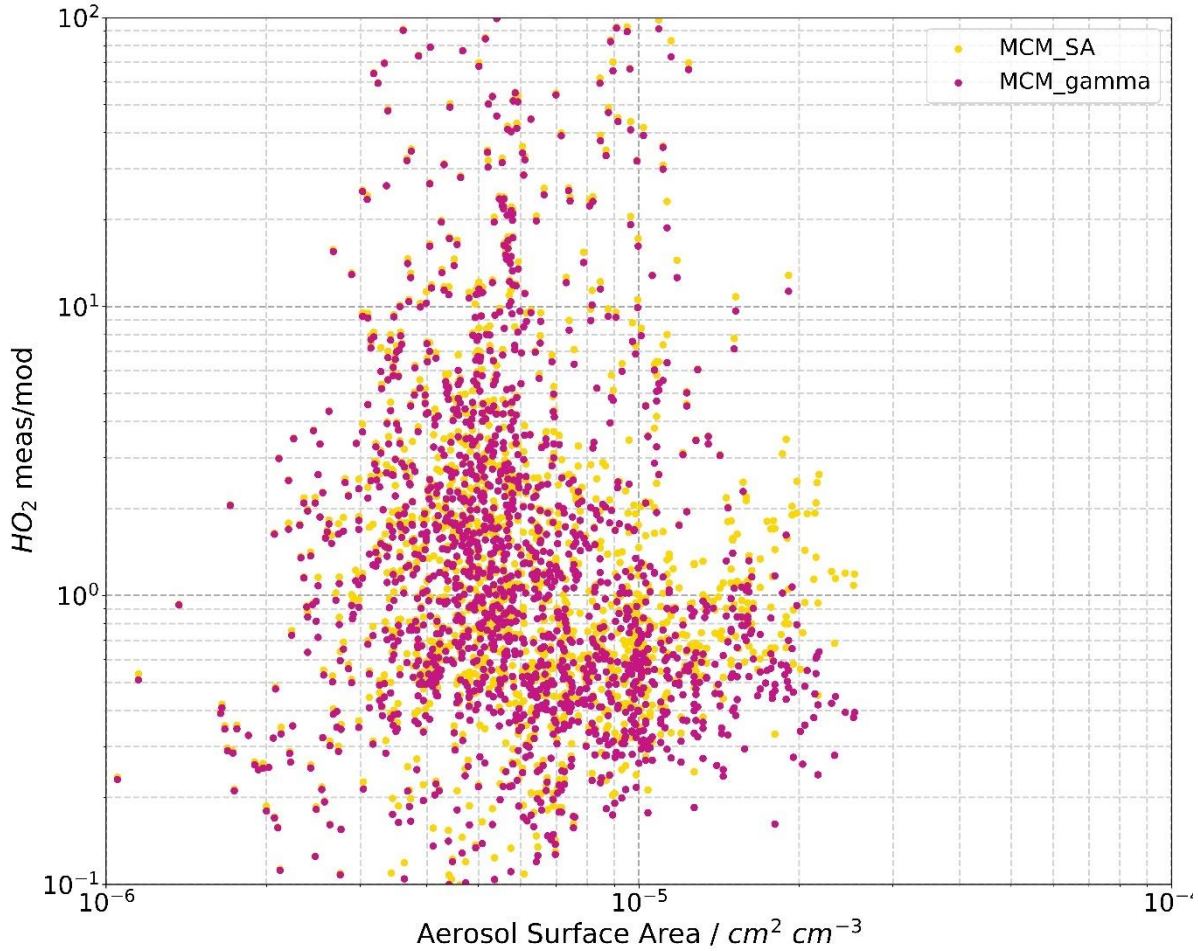

Figure S4. Ratio of measured to modelled HO_2 radical concentrations using the MCM_gamma (pink) and MCM_SA (yellow) models binned over the range of aerosol surface area concentrations (cm^2 cm^{-3}) for the summer AIRPRO campaign.

S1.5 Time series of absolute O_3 sensitivity across AIRPRO Summer campaign

The time series of absolute P(O_3), averaged up to a daily time resolution, across the entire measurement period is shown in Figure S5. Calculations of absolute O_3 production sensitivity showcase that for both MCM_gamma and MCM_SA, on average, the O_3 regime was VOC sensitive throughout the day with NO_x sensitivity increasing in the afternoons. As shown in Figure S6, when the NO mixing ratio was low and this coincided with high aerosol surface area, the O_3 sensitivity shifted from VOC to NO_x limited.

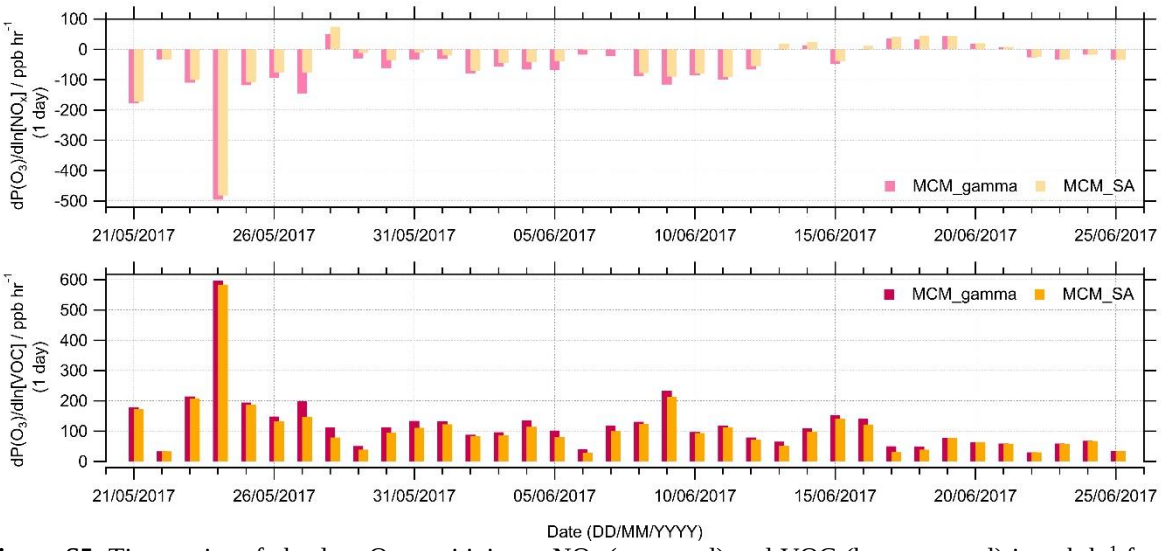

Figure S5. Time series of absolute O_3 sensitivity to NO_x (top panel) and VOC (bottom panel) in ppb h^{-1} for MCM_gamma (pink) and MCM_SA (yellow) averaged daily across the entire summer AIRPRO campaign. MCM_gamma includes γ_{HO_2} calculated using the Song parameterisation (av. 0.070 ± 0.035) while MCM_SA includes γ_{HO_2} at a fixed value of 0.2.

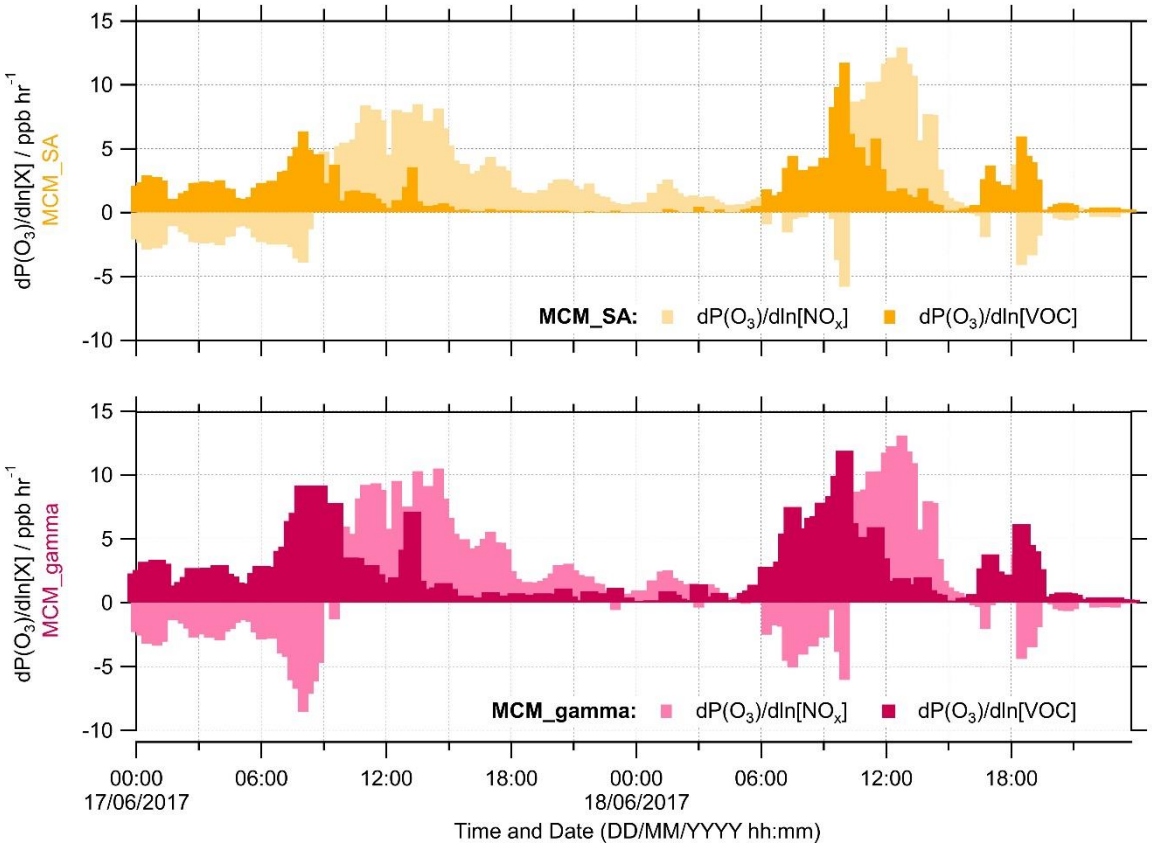

Figure S6. Time series of absolute O_3 sensitivity to NO_x (lighter shades) and VOC (darker shades) for MCM_SA (top panel) and MCM_gamma (bottom panel) for 17/06/2017-18/06/2017 showing an example where $dP(O_3)/dln[NOx] > dP(O_3)/dln[VOC]$ in the afternoon of both days. The average NO mixing ratio for this period was 0.41 ± 0.50 ppbV while the average SA concentration was (8.4 ± 6.2) × 10^{-6} cm^2 cm^{-3}. MCM_gamma includes γ_{HO_2} calculated using the Song parameterisation (av. 0.070 ± 0.035) while MCM_SA includes γ_{HO_2} at a fixed value of 0.2.

S1.6 Comparison of γ_{HO_2} for Beijing, 2017 and Wangdu, 2014 campaigns

In the Song et al., 2020, the γ_{HO_2} was calculated using measured data from a comprehensive 2014 field campaign at a rural site in Wangdu on the North China Plain. In Song et al., 2020, γ_{HO_2} was calculated as 0.116 ± 0.086 (for a_{HO_2} = 0.5) for the conditions of the Wangdu campaign. Another study by Tan et al., 2020 calculated the γ_{HO_2} value by comparing HO_2 field data with HO_2 modelled concentrations and estimating the HO_2 aerosol uptake coefficient required to close the radical budget for each day. This method lead to an average value of γ_{HO_2} = 0.08 ± 0.13 , within the uncertainty of the γ_{HO_2} value calculated by Song et al., 2020.

The average γ_{HO_2} value of 0.116 ± 0.086 for the Wangdu campaign is comparable, though slightly higher than the γ_{HO_2} value of 0.070 ± 0.035 calculated in this study for the summer AIRPRO Beijing campaign. A comparison of the measured parameters used within the Song parameterisation for both the Wangdu and Beijing campaigns are shown in Table S1.

Parameters	**Average Values for Wangdu**	**Average Values for Beijing**
ALWC (μg m^{-3})	68.2	6.94 (fixed as 14 in eqn 1)
Relative humidity (%)	61	43
[PM] (μg m^{-3})	67.2	38
[Cu]$_{eff}^{2+}$ (mol L^{-1}/ng m^{-3})	0.0005 / 35.8	0.0008 / 4
Count median radius, R_d (cm)	3×10^{-6}	1.5×10^{-6}

Table S1. Comparison of important measured parameters within the Song parameterisation for the Summer AIRPRO campaign in Beijing 2017 and the Wangdu campaign on the North China Plain, 2014. Wangdu campaign values from Song et al., 2020 and Song et al., 2022.

In the Song parameterisation, the uptake coefficient depends on [PM], [ALWC] and $[Cu^{2+}]_{eff}$, with the strongest dependence on $[Cu^{2+}]_{eff}$. As shown in Table S1**Table *S1***, both PM and ALWC concentrations were lower on average for the Beijing AIRPRO campaign compared to the Wangdu campaign. While the total copper mass concentration in ng m^{-3} was significantly lower (4 ng m^{-3} on average) for the Beijing campaign than the Wangdu campaign (35.8 ng m^{-3}), due to differences in the count median radius and aerosol volume, the $[Cu^{2+}]_{eff}$ calculated in mol L^{-1} was slightly higher for the Beijing campaign. This is due to a larger R_d value for the Wangdu campaign and therefore higher aerosol volume, due mostly likely in part to higher average RH across the campaign, which makes up for the difference in copper mass concentration between

the two campaigns. Comparable values of $[Cu^{2+}]_{eff}$, but lower [ALWC] and [PM] for the Beijing campaign explain why the estimated uptake coefficient values for Beijing are slightly lower than those for the Wangdu campaign.

References

Fuchs, H., Holland, F., and Hofzumahaus, A.: Measurement of tropospheric RO_2 and HO_2 radicals by a laser-induced fluorescence instrument, The Review of scientific instruments, 79, 084104, https://doi.org/10.1063/1.2968712, 2008.

Slater, E. J., Whalley, L. K., Woodward-Massey, R., Ye, C., Lee, J. D., Squires, F., Hopkins, J. R., Dunmore, R. E., Shaw, M., Hamilton, J. F., Lewis, A. C., Crilley, L. R., Kramer, L., Bloss, W., Vu, T., Sun, Y., Xu, W., Yue, S., Ren, L., Acton, W. J. F., Hewitt, C. N., Wang, X., Fu, P., and Heard, D. E.: Elevated levels of OH observed in haze events during wintertime in central Beijing, Atmos. Chem. Phys. Discuss., 2020, 1-43, https://doi.org/10.5194/acp-2020-362, 2020.

Song, H., Lu, K., Dong, H., Tan, Z., Chen, S., Zeng, L., and Zhang, Y.: Reduced Aerosol Uptake of Hydroperoxyl Radical May Increase the Sensitivity of Ozone Production to Volatile Organic Compounds, Environ. Sci. Tech. Letts., 9, 22-29, https://doi.org/10.1021/acs.estlett.1c00893, 2022.

Song, H., Chen, X., Lu, K., Zou, Q., Tan, Z., Fuchs, H., Wiedensohler, A., Moon, D. R., Heard, D. E., Baeza-Romero, M. T., Zheng, M., Wahner, A., Kiendler-Scharr, A., and Zhang, Y.: Influence of aerosol copper on HO_2 uptake: a novel parameterized equation, Atmos. Chem. Phys., 20, 15835-15850, https://doi.org/10.5194/acp-20-15835-2020, 2020.

Tan, Z., Hofzumahaus, A., Lu, K., Brown, S. S., Holland, F., Huey, L. G., Kiendler-Scharr, A., Li, X., Liu, X., Ma, N., Min, K.-E., Rohrer, F., Shao, M., Wahner, A., Wang, Y., Wiedensohler, A., Wu, Y., Wu, Z., Zeng, L., Zhang, Y., and Fuchs, H.: No Evidence for a Significant Impact of Heterogeneous Chemistry on Radical Concentrations in the North China Plain in Summer 2014, Environ. Sci. Technol., 54, 5973-5979, https://doi.org/10.1021/acs.est.0c00525, 2020.

Whalley, L. K., Stone, D., Bandy, B., Dunmore, R., Hamilton, J. F., Hopkins, J., Lee, J. D., Lewis, A. C., and Heard, D. E.: Atmospheric OH reactivity in central London: observations, model predictions and estimates of in situ ozone production, Atmos. Chem. Phys., 16, 2109-2122, https://doi.org/10.5194/acp-16-2109-2016, 2016.

Whalley, L. K., Stone, D., Dunmore, R., Hamilton, J., Hopkins, J. R., Lee, J. D., Lewis, A. C., Williams, P., Kleffmann, J., Laufs, S., Woodward-Massey, R., and Heard, D. E.:

Understanding in situ ozone production in the summertime through radical observations and modelling studies during the Clean air for London project (ClearfLo), Atmos. Chem. Phys., 18, 2547-2571, https://doi.org/10.5194/acp-18-2547-2018, 2018.

Whalley, L. K., Slater, E. J., Woodward-Massey, R., Ye, C., Lee, J. D., Squires, F., Hopkins, J. R., Dunmore, R. E., Shaw, M., Hamilton, J. F., Lewis, A. C., Mehra, A., Worrall, S. D., Bacak, A., Bannan, T. J., Coe, H., Ouyang, B., Jones, R. L., Crilley, L. R., Kramer, L. J., Bloss, W. J., Vu, T., Kotthaus, S., Grimmond, S., Sun, Y., Xu, W., Yue, S., Ren, L., Acton, W. J. F., Hewitt, C. N., Wang, X., Fu, P., and Heard, D. E.: Evaluating the sensitivity of radical chemistry and ozone formation to ambient VOCs and NOx in Beijing, Atmos. Chem. Phys. Discuss., 21, 2125-2147, https://doi.org/10.5194/acp-2020-785, 2021.

Woodward-Massey, R., Slater, E. J., Alen, J., Ingham, T., Cryer, D. R., Stimpson, L. M., Ye, C., Seakins, P. W., Whalley, L. K., and Heard, D. E.: Implementation of a chemical background method for atmospheric OH measurements by laser-induced fluorescence: characterisation and observations from the UK and China, Atmos. Meas. Tech., 13, 3119-3146, https://doi.org/10.5194/amt-13-3119-2020, 2020.